Limits of detection and precision for selected commercially available, low-cost carbon dioxide and methane gas sensors

Keywords: carbon dioxide; gas detectors; gas industry; methane; pollution measurement; sensor systems and applications

Word Count: 5,763

ABSTRACT

This manuscript examines several commercially available low-cost and low-power sensors to address their application for industrial and environmental monitoring. The objective is to assess their application in portable gas sensing equipment, and to advise sensor selection. For industrial monitoring, the eight-hour permissible exposure limit is 5,000 parts-per-million (ppm) for carbon dioxide and 1000 ppm for methane. For environmental monitoring, sensitivity close to the background is required, around 400 ppm for carbon dioxide and 0 ppm for methane. Using these limits, suitable sensors were selected based on market availability, cost, and power consumption. The resulting matrix of the limit of detection (LOD) and precision can be used to evaluate and select sensors for integration into a sensor platform for a specific application. The optical K-30 sensor from CO2Meter Inc. (LOD of 25 ppm, precision of 2 ppm) had one of the best cost to performance ratio for carbon dioxide. For methane, none of NDIR methane sensors were suitable for monitoring at the environmental concentration. The best cost to performance ratio for a methane sensor was the chemiresistive TGS-2611 sensor from Figaro Engineering Inc., which has a LOD of 16 ppm and precision of 0.2 ppm. However, this sensitivity comes at a loss of accuracy below 350 ppm due to non-linear response.

INTRODUCTION

The design of sensor platforms for real time monitoring of carbon dioxide and methane gas concentrations is of importance for environmental and industrial appli-

cations. For example, monitoring is essential to industries which utilize dry ice for packaging, and those with gas-based heating equipment. The eight-hour permissible exposure limit is 5,000 parts-per-million (ppm) for carbon dioxide and 1000 ppm for methane.[1,2] For typical monitoring applications, the sensor also need significant sensitivity close to the environmental background, 400 ppm for carbon dioxide[3,4] and 0 ppm for methane[5–7]. For enclosed environments found in industrial settings, the Hill and Smith review, along with the references contained within, provides an extensive review.[8] Likewise, the Tsai, Lin, and Chan review, along with included citations, provides an overview with respect to the office environments.[9] In settings where workers are likely to encounter high concentrations of dangerous gases, they are typically supplied a portable, personal air quality monitor. These devices are typically battery operated and must reliably sample the air while being constrained by their limited power supply. Thus, low-cost and low-power sensors are necessity (see Selection Criterion section for the authors' definition of these terms). For manufacturing and office spaces, personal monitoring equipment is normally not required. Instead, the entire space is monitored. For compliance, a collection of multiple samples at numerous locations in a given area is critical for effective sampling. An objective methodology for determining sensor distribution has been discussed Lui et al.[10] Other aspects of effective sampling, along with other considerations, are discussed by Keith et al.[11] Since these sampling strategies make use of distributed networks of small sensors instead of a single high-performance sensor, low-cost and low-power sensors are also required.

Applications for low-cost and low-power sensors include, but are not limited to, those used in HVAC air handlers,[12,13] chemical processing units,[14] oil well monitoring

devices,[15,16] and environmental monitoring.[17–21] In these applications, the designer must also take into account the limit of detection, precision, and accuracy for each sensor integrated within the unit. The limit of detection is the minimum concentration that can be detected as significantly different from the background.[22–24] Precision is the reproducibility of the measurement (defined here as the standard deviation of the response), while accuracy is how close the reported value is to the true value. Despite the large number of commercially available sensors and papers discussing their use in various applications, there is limited literature that directly compares limits of detection, precision, and accuracy of different sensor elements. One example of this informational availability which lacks comparison is a paper examining only the Figaro TGS 2600 methane sensor.[25] This scarcity of direct comparison hinders one's ability to select the optimal sensors for a sensor platform designed for a given application. A similar need for direct comparisons motivated a related study examining low-cost ozone, nitrogen dioxide, and carbon monoxide sensors.[26] Therefore, this study of commercially available low-cost and low-power sensors for carbon dioxide and methane was conducted under the same experimental conditions and using the same methodology to determine the limit of detection, precision, and accuracy. This study was performed under typical conditions required to ensure a safe environment, with respect to carbon dioxide and methane, in industrial and office settings.

METHODS

Low-Cost Sensing Methods

Currently available low-cost sensors can be categorized by detection method, for example optical absorption, chemiresistive,[27] and electrochemical. Since studies have cited concerns with electrochemical sensors, such as a short lifetime and lack of robustness,[28] only optical (carbon dioxide and methane) and chemiresistive sensors (methane) were selected for evaluation in this study. Although examples of chemiresistive carbon dioxide sensors have been reported in the literature, there are no commercially available devices known to the authors. Due to the practical focus of this study, only sensors which can easily be acquired by other researchers will be considered. It is generally accepted that optical sensors typically have excellent stability, selectivity, and fast response to concentration changes. Optical methods of detecting carbon dioxide and methane are based on measuring the absorption of light at $2352\,\mathrm{cm}^{-1}$ and $3015\,\mathrm{cm}^{-1}$, respectively.[29,30] Since these sensors rely on the Beer-Lambert law to relate absorption to concentration, the calibration is only dependent on the geometry of the sensor and physical properties of the gas.[31]

Lower cost optical sensors typically use nondispersive infrared (NDIR) sensing. This method uses a broad spectrum source of light which is restricted by a narrow band pass filter across the absorbance maximum before reaching the detector. As a result, lower cost parts can be used and the design can be both more compact and robust. In general, NDIR detection is used for carbon dioxide due to its large molar absorption coefficient, allowing for short path lengths to be used in devices. Methane is limited in practical applications due to its lower absorption coefficient and overlapping symmetric

C-H stretches. The overlapping stretches makes methane difficult to distinguish from other common aliphatic gases such as ethane and propane.[32] Although selectivity of the NDIR sensors with respect to different analyte gases was not explored in this study, it should be considered when these sensors are integrated into a monitoring device.

Chemiresistive sensors for detection of methane typically use a thin oxide film.[28] These sensors work by measuring resistance changes due to differences in the electron transport through the metal oxide film, in the presence of oxygen and reactive gases.[33] When the film is exposed to methane, the molecule adsorbs and reacts with surface oxygen species resulting in a change in the electrical conductivity.[34,35] Since the sensor depends on chemical reactions involving both atmospheric oxygen and methane for proper functioning, the measurement is dependent on the relative humidity, temperature, and film preparation. Chemiresistive sensors are known to respond to a range of hydrocarbon gases.[36] In many cases, the non-linear response curves for additional gases are included in the documentation provided by the manufacturer. However, similar to the optical sensors for methane, the selectivity was not explored but should be considered when integrating these devices into a sensor platform.

Selection Criterion

The selection of sensors was based on their cost and power consumption. The low-cost criterion is defined by the authors to be less than $100 (USD) per unit in bulk. However, the exact cost for each sensor will not be discussed in this paper to avoid price variability with time and vendor. Some exceptions were made to this low-cost requirement. In terms of cost, the optical Gascard sensors (sold by GHG Analytical) are an order of magnitude more expensive (thousands) than the other selected low-cost

sensors and requires additional pumping infrastructure to analyze gases. However, the typical bench-top instrument (such as the one used for measurement confirmation in this research) is another order of magnitude more expensive than the Gascard. The second-criterion is that the selected sensors can be used in portable low-power monitoring devices. While "low-power" is a subjective criterion, a definition similar to that provided by Karpov et al. is used.[37] This paper defines a low-power sensor as one capable of making two measurements per minute or two hours of continuous use on a battery pack of three AAA alkaline batteries (nominal capacity 4 W h). The selected metric as was chosen by the authors to limit the number of sensors for testing, and should not be interpreted as prescriptive for low-power sensors in general. Finally, the sensors selected, with two exceptions, were all commercially available in large quantities (at least 1000 units). Sensor availability is interpreted by the authors to be "able to be purchased commercially with sufficient units in stock."

Selected Sensors

In total, six carbon dioxide sensors were selected for testing, the K-30 SE-0018, COZIR AMB GC-020, Gascard CO_2, MSH-P/CO2/NC/5/V/P/F, MSH-DP/HC/CO2/NC/P/F, and Telaire T6615. For methane, seven sensors were evaluated, the MQ-4, Gascard CH_4, MSH-P/HC/NC/5/V/P/F, MSH-DP/HC/CO2/NC/P/F, TGS-2600, TGS-2610, and TGS-2611. Manufacturer information for each of the carbon dioxide and methane sensors is available in Table 1 and 2, respectively. The relevant properties for the carbon dioxide (Table S1) and methane sensors (Table S2), obtained from the manufacturer documentation), are summarized in the supplementary materials.

The K-30, COZIR, Dynament, and Telaire sensors are all NDIR carbon dioxide

sensors. Dynament also provides a dual gas NDIR sensor (MSH-DP/HC/CO2/) designed to measure both carbon dioxide and methane concentrations. This ability was attractive for applications requiring both low-cost and portability. The carbon dioxide and methane Gascard sensors were more expensive than the other chosen NDIR sensors. Their specifications combined with the included pressure and temperatures compensation make them attractive enough to compensate for the expense. In addition to the Gascard sensor, the Dynament hydrocarbon sensors (MSH-P/HC and MSH-DP/HC/CO2/) were chosen as inexpensive candidates for methane detection.

Selected chemiresistive sensors include the MQ-4 from Hanwei Electronics and TGS-2600, TGS-2610, and TGS-2611 manufactured by Figaro Engineering Inc. sensors. These low-cost methane sensors are typically used in gas warning systems.[38] The TGS sensors are used in commercial methane detectors, and the TGS-2600 sensor has been previously evaluated for atmospheric applications.[25,39] There are several different MQ versions optimized for hydrocarbon sensing. The MQ-4 sensor was chosen as this variant was specifically tuned for methane. Chemiresistive sensors required a minimum conditioning period or "burn-in" time. The "burn-in" time was met or exceeded for all chemiresistive sensors.

Analyte Gas Generation

To test these sensors under controlled conditions, a gas mixing apparatus (Figure 1) was constructed. An initial gas mixture (cylinder labeled "Calibrated Gas Mixture" in Figure 1) was further diluted using either purified air or nitrogen gas by a set of mass flow controllers to produce specific concentration of the analyte gases. The calibrated gas cylinders were supplied by Airgas Inc. (sourced from Tulsa, OK). Depending

on the specific experiment being performed, calibrated gas cylinders with different mixtures were used (See Table 3). In all cases, the calibrated gas concentrations were certified by Airgas, Inc. to be within ±2% of the stated values. Since the objective is to address the accuracy, precision, sensitivity, and limits of detection, only carbon dioxide and methane were used. However, selectivity requirements towards other gases must be considered when these sensors are integrated into a monitoring platform. For carbon dioxide experiments, the diluent or carrier gas (cylinder labeled "Carrier Gas" in Figure 1) was typically nitrogen. Using nitrogen as a carrier gas appropriately represents the bulk of air content with minimal potential contaminants. For methane, medical grade air (supplied by Airgas Inc., Tulsa, OK) was used as the carrier gas since the chemiresistive sensors required oxygen to correctly react with and measure the methane concentration. Medical grade air is free of contamination by particles, hydrocarbons and water.

The two flow controllers (Figure 1) are used to adjust the concentration of the analyte gas by varying the ratio of the calibrated gas to the carrier gas. The use of flow controllers, as opposed to valves, keeps the concentration of carbon dioxide and methane in the analyte gas constant for the duration of the experiment. Conservatively, concentration fluctuation induced by the two flow controller is 1% or less that the recored concentration values. The main uncertainty in the concentration of carbon dioxide and methane in the "Calibration Gas Mixture" cylinder provided by Airgas results in a systematic error. For atmospheric levels of carbon dioxide, the error is approximately 8 ppm. This error was determined by propagating the uncertainty in the calibrated gas cylinder supplied by Airgas Inc. for carbon dioxide by the appropriate

dilution factor. Around atmospheric levels of methane, the error in the concentration is less than 0.4 ppm. This limit was estimated from the uncertainty in initial calibrated gas cylinder for methane after dilution to 20 ppm or less. Since the fluctuations around the mean were independent of the exact concentration (see Precision and Baseline Noise Tests subsection), this systematic error will not affect the results from the baseline noise or the International Union of Applied Chemistry (IUPAC) limit of detection, discussed below. For the sensor calibrations, uncertainty in the absolute concentration of the "Calibration Gas Mixture" cylinder will introduce an offset in the intercept but not the slope.

A high-quality bench-top analyzer (ZRE Non-Dispersive Infrared Analyzer, California Analytical Instruments, Inc., Orange, CA), sensitive to both carbon dioxide and methane, was used as a precision reference. The solenoid valves in the gas mixing apparatus were used to send either gas from the "Carrier Gas" cylinder to provide a zero reference or from the undiluted "Calibration Gas Mixture" cylinder (provided by Airgas, Inc.) to the analyzer to calibrate the span. Calibration of the bench-top analyzer was performed as per the manufacturerś recommendation and concentration values were recorded from the screen. Thus, the ranges and all reported concentration values in this article are not whole numbers, but measured valves.

Controlled Gas Exposures

Multiple sensors were operated concurrently as shown in Figure 2 (data collection described in the Data Collection section. The "Gas Mixer" in this diagram is the gas mixing apparatus shown in Figure 1, and the "Gas Analyzer" is the ZRE Non-Dispersive Infrared Analyzer, California Analytical Instruments, Inc., Orange, CA.

There are two types of gas sampling methods used by the selected sensors, diffusion (the sensor samples the gas surrounding a sensing element) and flow (the sensor has an internal volume with the gases must flow through). The method used for each sensor is summarized in Table S1 and S2 in the supplemental. In the experimental setup (Figure 2), the flow capable sensors were connected directly to gas flow from the mixing apparatus. The diffusion sampling sensors are contained within in the "Sensor Flow Box" enclosures or in the larger "Gas Flow Chamber" enclosure depicted in Figure 2. "Sensor Flow Box" enclosures contained the K-30 carbon dioxide sensor and a socketable chemiresistive methane sensor (such as the MQ-4 or TGS series sensors). The larger "Gas Flow Chamber" contained the COZIR, Telaire, Dynament, and K-30 sensors. Given the large total volume, data collected from the sensors in this chamber were analyzed only after the system reached a constant concentration following the introduction of a gas with known concentration of carbon dioxide or methane. In some experiments, performed to accurately measure the response time for chemiresistive sensors, a smaller sensor enclosure (internal volume 2.54 cm^3) was used to minimize the time to reach a stable concentration.

Data Collection

$$\varsigma = \frac{V_{measured}}{V_{cc} - V_{measured}} \times \frac{1}{R_{ref}} \tag{1}$$

.

For each sensor, data was collected using evaluation hardware and software from sensor manufacturers when available, or lab-built electronics (based on Arduino mi-

crocontroller board) per manufacturer recommendations. Due to the unique interface requirements of each sensor, development kits were purchased when possible. Measurement frequency is dependent on the capabilities of the hardware and software provided by the manufacturer and type of experiment being performed. In general, all measurements were made at a rate of one measurement per second or faster. The chemiresistive sensors were energized using the recommended voltage for the heater element and the response was measured using a 12-bit A/D converter, after buffering and filtering, across a reference resistor (a 10 kΩ resistor was used for R_{ref}). The A/D converter was referenced using the 5V supply, which was also connected to the sensing element of the chemiresistive sensor. Equation 1 describes the conversion of the measured voltage ($V_{measured}$) to the conductivity (ς), measured in Siemens (S).

Data Collection for Sensor Calibration

Calibration curve of each sensor was determined by varying concentrations and recording the output. The carbon dioxide sensors were calibrated using gas concentrations from 34.5 to 1020 ppm. The lower range was to determine the limit of detection while the larger range is close to the eight-hour permissible exposure limit. For the methane sensors, most calibration curves were generated from gas concentrations between 1.85 and 995 ppm. This range is consistent with less than 0 ppm experimental concentration for methane in the environment to the eight-hour permissible exposure limit of 1000 ppm. During the generation of a typical calibration curve, concentration data from each sensor was continually collected (see the Data Collection section). For each point, the carrier gas was first introduced. Once a stable response was measured for each sensor, the carrier gas was obtained. A analyte gas at a known concentration (see

the Analyte Gas Generation section) introduced to the testing chamber, and after 20 to 30 hours, it was turned off. This long collection time was not required to obtain precise reading of the concentration by each sensor. However, the collection time was chosen to ensure that significant number of data points were generated to allow a detailed study of the fluctuations around the mean value (see the Data Collection for Baseline Noise Determination section). The pure carrier gas was reintroduced, and the system was allowed to stabilize before the next measurement. Since the concentration data from each sensor was continually collected, the average baseline and response to each gas concentration can be extracted. The average response at each concentration was determined from the data collected after the system stabilized (including any overshoot or ringing). After data collection, the average responses at each concentration, after background correction if required, were plotted and fitted to a response model.

Data Collection for Baseline Noise Determination

For the baseline noise determination, data collection was preformed around the baseline atmospheric concentration for each analyte gas, which is approximately 400 ppm for carbon dioxide[3,4] and under 2 ppm for methane.[5–7]. During the procedure, concentration data from each sensor were continually collected (see the Data Collection section). First the carrier gas was introduced. After stable response was measured for each sensor, the analyte gas (400 ppm for carbon dioxide and 0 ppm for methane) was introduced to the testing chamber. After 20 to 30 hours, the data collection was stopped. The need for a long collection time is discussed in Precision and Baseline Noise Tests section.

RESULTS AND DISCUSSION

Sensor Response

To provide an example of the data collected from the sensors, Figure 3 shows the response of two selected carbon dioxide sensors, the K-30 and Gascard, to 600 and 1400 concentration steps of carbon dioxide. The K-30 reports the concentration directly, while the Gascard reports a digital value between zero and one, with one being the maximum concentration (30,000 ppm carbon dioxide for the sensor used in this study). This calibration was applied to the output of the Gascard before plotting. Both optical sensors respond very quickly to an increase in carbon dioxide inside the environmental chamber. The data demonstrate relative similarity in behavior of the selected sensors in the presence of concentration changes well above the limit of detection.

The measured response times for the chemiresistive sensors were determined by the change in conductivity of the sensor. Figure 4 depicts a plot of the temporal response of an MQ-4 sensor to five different concentrations of methane between 500 and 2200 ppm, which could represent a methane leak. The sensor produces significant overshoot, often exceeding 100% of the final response. Normally, sensors are characterized by rise time or the time required for the response to change from 10% of the baseline value to 90% of the mean response. Given the overshoot, the settling time (the time required to reach steady state after a concentration change) is more useful. For all concentrations, a stable value within 2.5% of the mean was produced after 78±10 s, when averaged over all experiments. The settling time for the MQ-4 sensor did not appear to be concentration dependent. The observed overshoot may be a result of a complex set of chemical reactions at differing rates occurring on the surface as the system reaches a new steady

state response after a change. In addition, some of the overshoot could be a result of the small interruption in the gas flow during a concentration change. The MQ-4 sensors are the worst case, the TGS sensors produced less overshoot and a faster settling time.

It is important to note that all responses have been processed by the internal electronics in these sensors when available. For example, the K-30 has an internal sampling rate of 2 seconds. The chemiresistive sensors responded on a notably different timescale than the optical sensors, as seen by comparing the step response in Figure 3 to that in Figure 4. In environmental monitoring application, the power requirement may require in these sensors to be periodically turned on and off. This power cycling will further increase the response time due to the thermal heating of the sensing element.

Carbon Dioxide Sensor Calibrations

Calibration curves were determined by varying concentrations and recording the output, as discussed in Data Collection for Sensor Calibration section. The average responses at each concentration, after background correction if required, were plotted and fitted. Consistent with the Beer-Lambert law, the measured response (absorbance) from all sensors as a function of the carbon dioxide concentration showed a linear response. Linear regression was used to determine the calibration and standard error. Example calibration plots for an optical sensors are shown in the top panel of Figure 5. The data points are the measured values from each sensor at each concentration, while the line is a linear fit to the data. The gap in ppm is due to different concentrations of the calibration gas used for the low and high ranges. The low range is important for the limit of detection calculation, while the high range reflects the recommended concentration range. Since the calibration curves were produced with respect to the

calibrated California Analytical Instruments Inc. ZRE (see Sensor Calibration subsection), these curves provide an estimate of the accuracy of the sensor. In general, it was found that all of the sensors must be calibrated before deployment, rather than used directly from the supplier. With the exception of the carbon dioxide Gascard sensor, there was poor accuracy without an initial calibration. These optical sensors could be easily recalibrated, and the calibration stored on the device. The measured linear calibration curves for the optical carbon dioxide sensors all have slopes close to one another with respect to the known carbon dioxide concentrations. This result is expected as the slope is determined by the optical path length and the physical properties of the analyte. Thus, the inaccuracy is primary in the value of the vertical intercept, or the value of zero concentration. To address this issue, a majority of the optical sensors tested provide an easy way to adjust the intercept to zero using the known average background level of carbon dioxide to provide reasonable and practical reference.

Methane Sensor Calibrations

The calibration data was collected using the methodology used for carbon dioxide discussed above Data Collection for Sensor Calibration section). Again, the average responses at each concentration, after background correction if required, were plotted and fitted. The optical methane Gascard sensor provide the expected linear response and good accuracy without an initial calibration. For the a typical chemiresistive methane sensor, the calibration plots is shown in the bottem panel of Figure 5. This plot is similar to calibration plots from chemiresistive sensor manufacturers, which typically start around 200 to 300 ppm. The data in this study below 100 ppm shows significant variation, indicative of these concentrations are below the limit of detection. The larger

variation at low concentrations seen in the plot of MQ-4 conductivity is also consistent with measurements of the baseline fluctuations of these sensors with time.

All chemiresistive sensors produced non-linear calibration curves. Data sheets from the MQ-4 and TGS sensors showed significant non-linearity, especially at low concentrations. All chemiresistive sensors show a rapid increase in conductivity during exposure to low concentrations of gas, which exacerbates any measurement at these low levels. The response curve was modeled using a Langmuir-like or Langmuirian form, which provided a response consistent with that specified by the manufacturer. Additional dependences of the output with ppm have been suggested by kinetic analysis.[40,41] One notable function is a power law model, where the log of the output is proportional to the log of the ppm between 200 and 10,000 ppm. For the 200 and above ppm range, acceptable results were obtained. However, this model produced a calibration curve which increased too rapidly with ppm at lower concentration. Furthermore, the power law relationship increases monotonically with concentration, and does not accurately model a real sensor where the response, limited by the surface reactions, should become constant at high concentrations. Thus, a Langmuir form shown in Equation 2 provided a simple fit, and produced a well behaved linear dependency as the ppm approaches zero. The valve of a represents the asymptotic valve at high concentrations, while a times b determines the linear dependency at low concentrations. The valves of a and b, along with the asymptotic standard errors, were determined by fitting the experimental data using the Levenberg-Marquardt algorithm in *gnuplot*.[42]

$$f(x) = \frac{a \times b \times x}{1 + b \times x} \tag{2}$$

Multiple MQ-4 chemiresistive sensors under similar conditions showed significant differences in the calibration parameters. Unlike optical sensors for carbon dioxide which typically only needs the zero (reading at zero ppm) reestablished, chemiresistive sensors require the measurement of a complete non-linear calibration curve to ensure precision. The output of the chemiresistive sensors are also dependent on temperature and humidity, further hampering this process.[43] For many chemiresistive sensors, the expectation of good accuracy with time may be impractical without repeated recalibration.

Precision and Baseline Noise Tests

The measurement baseline noise of each sensor was performed as described in the Data Collection for Baseline Noise Determination section. In most cases, the baseline of the sensors was determined by a 20 to 30 hour data collection time at a known concentration (400 ppm for carbon dioxide and 0 ppm for methane based on previously discussed atmospheric baselines) under a uniform flow. These long measurement times were required to fully capture the distribution of the output of each sensor around the mean. Collection times were adjusted to ensure that significant data points in the tails of the expected Gaussian distribution around the mean were recorded. The precision was determined by Gaussian characterization of the data collected during both calibration runs and the baseline experiments. In general, the optical sensors displayed flat baselines. Chemiresistive sensors typically display baseline changes due to humidity and temperature, which must be taken into account in monitoring applications. Figure 6 shows a typical data set for the TGS-2611 and MQ-4 sensor. TGS-2611 sensor displayed significantly less baseline drift than the MQ-4 sensor.

Since the initial Fourier analysis showed no significant periodic variations, distribution of the digitized sensor output around the mean response of the sensor was used to quantify the precision and baseline noise. The data stream (sensor output with time) from each sensor was subtracted from the mean response of the sensor, and a histogram of these differences was created. Since the digitized sensor outputs have a finite number of possible output values, no additional bins were created while producing the analysis. Although the data used for this analysis was obtained at typical environmental concentrations, additional experiments found that the measured deviation around the mean for each sensor was independent of the concentration of analyte gas. There was insignificant correlation between the concentration of the analyte gas and the σ obtained at each concentration, as quantified by the Pearson's Correlation Coefficient ($\rho = -0.173$).

The resulting histograms, along with a best-fit Gaussian peak, are shown in Figures. 7 and 8 for the carbon dioxide and methane sensors, respectively. In Table 4, σ_{GAUSS} is the standard deviation determine from the Gaussian fit. The standard deviation (σ) calculated from the background subtracted sensor data is almost identical to σ_{GAUSS}. In Figures. 7 and 8, the abscissa (x−coordinate) was scaled by the standard deviation of the data set and the area normalized to one. The resolution of the dual gas Dynament (MSH-DP/HC/CO2) sensor was insufficient to properly determine the fluctuations around the mean, as this sensor only reported two values with time at the given concentration. The result is consistent with the resolution stated in their documentation which lists 0.01% or 100 ppm as the low end of the concentration range. The fluctuation around the mean for the single gas Dynament (MSH-P/CO2) sensor is slightly less that the stated resolution of 50 ppm.

To determine the quality of the Gaussian fits in Figures. 7 and 8, the root-mean-squared error (RMSE) between the fit and the experimentally generated histogram was calculated for each sensor. These values are also listed in Table 4. For RMSE, a lower value indicates that the Gaussian function fits closely to the data points, whereas a higher value indicates a poorer fix. The values listed in Table 4 range from roughly 0.150 to 0.300. As the probability density function to which the data were fit was normalized to 1, the RMSE values are unitless. Since RMSE is a measure of fit, these values can be used in conjunction with σ_{GAUSS} to characterize the sensors.

Of the carbon dioxide sensors (see Figure 7 and Table 4), the Gascard and K-30 sensors produced the smallest standard deviation around the mean, σ_{GAUSS}, or the highest precision. The σ_{GAUSS} value of the Telaire sensor was approximately 2 times than that of either the Gascard or the K-30 sensor. The COZIR and Dynament (MSH-P/CO2/) sensors generated σ_{GAUSS} values which were significantly greater than that of the Gascard, Telaire and K-30 sensors. Finally, the dual gas Dynament (MSH-P/HC/CO2/) sensor produced the largest deviation from the mean. The fluctuations around the mean is slightly lower than the quoted resolutions in the manufacturer's documentation of 50 and 100 ppm, respectively, for these two sensors.

The Gascard sensor for carbon dioxide produced a normal response around the mean detected value with low RMSE. At times, there were some large fluctuations, several standard deviations around the mean response, in the output of the Gascard. This suggests that some minimal digital filtering may be required. For the K-30 sensor, a good Gaussian fit was produced (small RMSE). However, the distribution for the K-30 was skewed toward higher concentration values and appears to contain two

overlapping peaks. This causes the σ_{GAUSS} to be slightly larger and the RMSE to be artificially inflated. Careful analysis of this double peak shows that each peak has a similar standard deviation (σ), suggesting a small shift in the mean measured value. Since the K-30 sensor periodically adjusts for changing backgrounds in the firmware to ensure a normal output concentration of 400 ppm, the observed change in the reported mean concentration in the middle of the run is likely caused by this period background adjustment. It is also possible that periodic temperature and pressure variations, which are corrected for by the Gascard sensor, are responsible for the observed skew in the K-30. In general, precise work requires incorporation of pressure and temperature sensors into potential environmental sensing units to allow ppm corrections to be performed at time of measurement.

The probability distribution of responses around the mean by the GE Telaire sensor is a single peak with a σ_{GAUSS} that is approximately 2 to 3 times as large as that of the K-30 and Gascard sensors. Since the GE Telaire and K-30 sensor share comparable sensing mechanisms and path lengths, this larger σ_{GAUSS} was initially surprising. A direct comparison of the response for both the Telaire and K-30 sensors both with and without ambient light, showed that, unlike the K-30 sensor, the Telaire sensor was sensitive to ambient light level. Given that long data collection times are required to produce reliable histograms, the ambient light conditions changed over the course of data collection. It was suspected that the larger deviations around the mean for the Telaire sensor and resulting σ_{GAUSS} values are due to changes in the ambient light. Further experiments running the Telaire sensor in an enclosure under darkness proved this suspicion to be true.

For the optical methane sensors (see Figure 8 and Table 4), the Gascard for methane produced a σ_{GAUSS} with a low RMSE. The single gas Dynament (MSH-P/HC/) hydrocarbon sensor produced a very low σ_{GAUSS} and performed well in terms of precision. For this sensor, the 3.54 ppm precision (σ_{GAUSS}) is lower than the 50 ppm resolution quoted in the manufacturer's documentation at the low-end of the 1% concentration range of the sensor. However, the IUPAC limit of detection, discussed below, is consistent with the 50 ppm resolution. The σ_{GAUSS} for the dual-gas Dynament (MSH-DP/HC/CO2/) sensor was not included in this table. As mentioned previously, the dual-gas Dynament (MSH-DP/HC/CO2/) sensor only reported two values for methane around the mean rather than a distribution of several values. This result is also consistent with the 100 ppm resolution quoted in the manufacturer's documentation for concentrations of less than 10% methane.

The result for the chemiresistive methane sensors are also shown in Figure 8, with a σ_{GAUSS} and a RMSE results in Table 4. The distribution curve for the MQ-4 sensor was not included. Since the MQ-4 sensor displayed significant baseline drift when compared to the TGS-2611 sensor (Figure 6), the standard deviation was instead calculated directly from a relatively flat region of the baseline. This different treatment is not inconsistent with the use of the sensor in many applications where drift is a result of temperature and humidity. Previous studies by Solis et al. have shown noise produced by chemiresistive sensors, specifically the TGS-26XX series of sensors, is temperature dependent.[44] In general, the use of a dynamic background subtraction algorithm is required for the performance of chemiresistive. The σ_{GAUSS} results of the TGS-2600 and TGS-2610 were similar, as expected due to their similar sensing mechanisms. The baseline noise,

as quantified by σ_{GAUSS}, for the methane optimized TGS-2611 sensor was lower than the other TGS sensors.

Limits of Detection

As noted in the introduction, the limit of detection is the minimum concentration that can be detected as significantly different from the background.[22–24] IUPAC defines the limit of detection as three times the standard deviation (σ) from the background. For the sensors discussed here, the raw output from the sensors must be transformed into concentration value, and any error in the calibration will affect the limit of detection. For measurements requiring a calibration curve, Long and Winefordner provide a review of the various definitions as well as several examples.[22] For a linear calibration, the procedure to calculate the limit of detection is straightforward.[22] For optical sensors, the limit of detection can be calculated from the errors in the slope and intercept as obtained by the calibration curve (see Sensor Calibration subsection). For the non-linear chemiresistive sensors, error propagation can also be used to determine the limit of detection. Given the non-linearity and steepness of response (change in resistance vs ppm) of the chemiresistive sensors at the detection limit, the limit of detection determined by 3σ without correction for error in the calibration curve can be significantly different than that determined after correction (see Long and Winefordner discussion of the limit of detection definition).[22]

The limits of detection were computed from the σ_{GAUSS} discussed in the Data Collection for Baseline Noise Determination section and are listed in Table 5. The corrected limits of detections were determined after applying a correction based on the errors in the calibration curves.[22] It should be noted these tests were carried out in a

controlled environment and are best-case values. Of the tested carbon dioxide sensors, the Gascard and K-30 have the lowest limits of detection. The Telaire sensor also shows a comparable limit of detection. These results are consistent with expectations based on the longer path lengths of the sensors. The COZIR and Dynament single analyte sensor (MSH-P/CO2/) have the next highest limit of detection, and the Dynament dual analyte sensor (MSH-DP/HC/CO2) has the highest. These results reflect the ordering of σ_{GAUSS} in Table 4.

The limit of detection for the Dynament single analyte sensor (MSH-P/HC/) for methane demonstrates the important influence of the calibration curve on the reported error. This sensor has a stated resolution of 50 ppm by the manufacturer. This resolution was reflected by the standard errors in the slope and intercept.[22] After correcting for the calibration curve error, the limit of detection is three times the stated resolution. Thus, the calibration corrected limit of detection is consistent with the expectations of the manufacturers. However, the value produced by the IUPAC method, directly multiplying the standard deviation of responses, is 15 times lower. While this much lower number is correct, it only reports the digitization error of the electronics, and does not produce a meaningful limit of detection for the sensor. This illustrates the necessity of determining the error in the calibration curve.

Of the tested chemiresistive methane sensors, the TGS-2611 sensor had the lowest limit of detection under controlled conditions, primarily due to its stable baseline which influences both the background noise and the quality of the calibration. Similar sensitivities have been reported for the TGS-2600.[25] Both the non-methane optimized TGS-2600 and TGS-2610 sensors had similar limits of detection which were slightly

larger than the methane optimized TGS-2611 and the MQ-4. The MQ-4 sensor has performance between the TGS-2611 and both the TGS-2600 and TGS-2610 sensors. The 82 ppm limits of detection for the MQ-4 sensor is consistent with scatter in the calibration curve at concentration under 100 ppm (see Figure 4).

CONCLUSION

The detection limits, accuracy, and precision for a range of potential sensors for measuring ppm concentrations of carbon dioxide and methane for low-cost monitoring instrumentation were quantified the baseline atmospheric concentration, approximately 400 ppm for carbon dioxide[3,4] and under 2 ppm for methane.[5–7] The selected sensors were also evaluated at gas concentrations exceeding 1000 ppm to examine concentrations close to the permissible exposure limits. For carbon dioxide, the Gascard sensor had high performance based on the standardization and the limit of detection reported in Tables 4 and 5, but is comparatively more expensive than the other sensors investigated. The Gascard is limited by reliance on active sampling which requires a pump that introduces a source of additional power consumption, a mechanical failure point, and sampling complexity. Since concentrations are parts-per notation, the inclusion of temperature and pressure corrections on the Gascard is useful to automatically correct for these values. Thus, this sensor eliminates the need for additional sensors for precise measurements. Both the K-30 and Telaire sensors had good performance. The ability of the K-30 and Telaire sensors to operate by passive diffusion rather than mechanically pumped flow also reduces the cost and complexity of a potential monitoring system.

With respect to the measured LOD and precision, the K-30 sensor from CO2Meter Inc. had a limit of detection of 25 ppm, and a precision and accuracy (after calibration) of 2 ppm. The K-30 sensor also has the option to auto-zero by assuming that the minimum concentration of a multi-day run is 400 ppm, if used properly, this feature has advantages for remote instrumentation.

For methane, all sensors provided adequate sensitively at the permissible exposure limit of 1000 ppm, and most provide warning at one-tenth of this level. For environmental monitoring, there is no single sensor which meets ppm sensitivity required at atmospheric concentration (2 ppm). The limit of detection for the selected relativity low-cost optical methane sensors reported in Table 5 collectively show that these NDIR sensors are not suitable for monitoring environmental levels of methane around the global average. The best chemiresistive sensor for methane was the TGS-2611 sensor from Figaro Engineering Inc. This sensor has a limit of detection of 16 ppm and precision of at least 0.2 ppm. However, at the lower ppm (less than 350 ppm) the accuracy was poor due to the non-linear response. Although progress has been made to produce viable methane sensors,[30] larger, more costly devices are still required for environmental measurements at the ppm level.

REFERENCES

[1] **Centers for Disease Control**: Centers for Disease Control - National Institute for Occupational Safety and Health - Carbon Dioxide, https://www.cdc.gov/niosh/npg/npgd0103.html (2016).

[2] **Centers for Disease Control**: Centers for Disease Control - National Institute for Occupational Safety and Health - Methane (2015).

[3] **Blasing, T.**: Recent Greenhouse Gas Concentrations, Technical report, U. S. Department of Energy, CDIAC (2016).

[4] **Dlugokencky, E.**: Trends in Atmospheric Methane, Technical report, NOAA/ESRL (2016).

[5] **Turner, A. J.**, **D. J. Jacob**, **J. Benmergui**, **S. C. Wofsy**, **J. D. Maasakkers**, **A. Butz**, **O. Hasekamp**, and **S. C. Biraud**: A large increase in U.S. methane emissions over the past decade inferred from satellite data and surface observations, *Geophysical Research Letters 43*(5):2218–2224 (2016).

[6] **Bamberger, I.**, **J. Stieger**, **N. Buchmann**, and **W. Eugster**: Spatial variability of methane: Attributing atmospheric concentrations to emissions, *Environmental Pollution 190*:65–74 (2014).

[7] **Dlugokencky, E.** and **P. Tans**: Trends in Atmospheric Carbon Dioxide, Technical report, NOAA/ESRL (2016).

[8] **Hill, R. J.** and **P. A. Smith**: Exposure assessment for carbon dioxide gas: Full shift average and short-term measurement approaches, *Journal of Occupational and Environmental Hygiene 12*(12):819–828 (2015). PMID: 26023742.

[9] **Tsai, D.-H.**, **J.-S. Lin**, and **C.-C. Chan**: Office workers' sick building syndrome and indoor carbon dioxide concentrations, *Journal of Occupational and Environmental Hygiene 9*(5):345–351 (2012). PMID: 22530709.

[10] **Liu, M. K.**, **J. Avrin**, **R. I. Pollack**, **J. V. Behar**, and **J. L. McElroy**: Methodology for designing air quality monitoring networks: I. theoretical aspects, *Environmental Monitoring and Assessment 6*(1):1–11 (1986).

[11] **Keith, L. H.**, **W. Crummett**, **J. Deegan**, **R. A. Libby**, **J. K. Taylor**, and **G. Wentler**: Principles of environmental analysis, *Analytical Chemistry 55*(14):2210–2218 (1983).

[12] **Yang, Z.**, **N. Li**, **B. Becerik-Gerber**, and **M. Orosz**: A systematic approach to occupancy modeling in ambient sensor-rich buildings, *SIMULATION 90*(8):960–977 (2014).

[13] **Chung, W.-Y.** and **S.-C. Lee**: A selective AQS system with artificial neural network in automobile, *Proceedings of the Eleventh International Meeting on Chemical Sensors IMCS-11IMCS 2006IMCS 11 130*(1):258–263 (2008).

[14] **Won, W.** and **K. S. Lee**: Nonlinear observer with adaptive grid allocation for a fixed-bed adsorption process, *Computers & Chemical Engineering 46*:69–77 (2012).

[15] **Yi, P.**, **L. Xiao**, and **Y. Zhang**: Remote real-time monitoring system for oil and gas well based on wireless sensor networks, in Mechanic Automation and Control Engineering (MACE), 2010 International Conference On, 2427–2429, 2010.

[16] **Somov, A.**, **A. Baranov**, **D. Spirjakin**, **A. Spirjakin**, **V. Sleptsov**, and **R. Passerone**: Deployment and evaluation of a wireless sensor network for methane leak detection, *Selected Papers from the 26th European Conference*

on Solid-State Transducers Kraków, Poland, 9-12 September 2012 202:217–225 (2013).

[17] **Pering, T.**, **G. Tamburello**, **A. McGonigle**, **A. Aiuppa**, **A. Cannata**, **G. Giudice**, and **D. Patanè**: High time resolution fluctuations in volcanic carbon dioxide degassing from Mount Etna, *Journal of Volcanology and Geothermal Research 270*:115–121 (2014).

[18] **Black, R.**, **C. (Mick) Meyer**, **A. Yates**, **L. V. Zweiten**, and **J. Mueller**: Formation of artefacts while sampling emissions of PCDD/PCDF from open burning of biomass, *Chemosphere 88*(3):352–357 (2012).

[19] **Guohua, H.**, **W. Lvye**, **M. Yanhong**, and **Z. Lingxia**: Study of grass carp (Ctenopharyngodon idellus) quality predictive model based on electronic nose, *Sensors and Actuators B: Chemical 166–167*:301–308 (2012).

[20] **Karunanithi, S.**, **N. M. Din**, **H. Hakimie**, **C. K. Hua**, **R. C. Omar**, and **T. C. Yee**: Performance of labscale solar powered wireless landfill monitoring system, in Energy and Environment, 2009. ICEE 2009. 3rd International Conference On, 443–448, 2009.

[21] **Shendell, D. G.**, **J. H. Therkorn**, **N. Yamamoto**, **Q. Meng**, **S. W. Kelly**, and **C. A. Foster**: Outdoor near-roadway, community and residential pollen, carbon dioxide and particulate matter measurements in the urban core of an agricultural region in central CA, *Atmospheric Environment 50*:103–111 (2012).

[22] **Long, G. L.** and **J. D. Winefordner**: Limit of Detection A Closer Look at the IUPAC Definition, *Analytical Chemistry 55*(07):712A–724A (1983).

[23] **Currie, L. A.**: Detection: International update, and some emerging di-lemmas involving calibration, the blank, and multiple detection decisions, *Chemometrics and Intelligent Laboratory Systems 31*(1):151–181 (1997).

[24] **Mocak J.**, **Bond A. M.**, **Mitchell S.**, and **Scollary G.**: A statistical overview of standard (IUPAC and ACS) and new procedures for determining the limits of detection and quantification: Application to voltammetric and stripping techniques (Technical Report), *Pure and Applied Chemistry 69*(2):297 (2009).

[25] **Eugster, W.** and **G. W. Kling**: Performance of a low-cost methane sensor for ambient concentration measurements in preliminary studies., *Atmospheric Measurement Techniques 5*(Copyright (C) 2015 American Chemical Society (ACS). All Rights Reserved.):1925–1934 (2012).

[26] **Afshar-Mohajer, N.**, **C. Zuidema**, **S. Sousan**, **L. Hallett**, **M. Tatum**, **A. M. Rule**, **G. Thomas**, **T. M. Peters**, and **K. Koehler**: Evaluation of low-cost electrochemical sensors for environmental monitoring of ozone, nitrogen dioxide, and carbon monoxide, *Journal of Occupational and Environmental Hygiene 15*(2):87–98 (2018). PMID: 29083958.

[27] **Wetchakun, K.**, **T. Samerjai**, **N. Tamaekong**, **C. Liewhiran**, **C. Siriwong**, **V. Kruefu**, **A. Wisitsoraat**, **A. Tuantranont**, and **S. Phanichphant**: Semiconducting metal oxides as sensors for environmentally hazardous gases, *Sensors and Actuators B: Chemical 160*(1):580 – 591 (2011).

[28] **Neri, G.**: First Fifty Years of Chemoresistive Gas Sensors, *Chemosensors 3*(1):1–20 (2015).

[29] **Frodl, R.** and **T. Tille**: A High-Precision NDIR Gas Sensor for Automotive Applications, *IEEE Sensors Journal 6*(6):1697–1705 (2006).

[30] **Zhu, Z.**, **Y. Xu**, and **B. Jiang**: A One ppm NDIR Methane Gas Sensor with Single Frequency Filter Denoising Algorithm, *Sensors (Basel, Switzerland) 12*(9):12729–12740 (2012).

[31] **Bacsik, Z.**, **J. Mink**, and **G. Keresztury**: FTIR Spectroscopy of the Atmosphere. I. Principles and Methods, *Applied Spectroscopy Reviews 39*(3):295–363 (2004).

[32] **Coblentz Society, Inc.**: Evaluated Infrared Reference Spectra, in NIST Chemistry WebBook (P. J. Lindstrom and W. G. Mallard, eds.), number 69 in NIST Standard Reference Database, Gaithersburg MD, 20899: National Institute of Standards and Technology.

[33] **Albert, K. J.**, **N. S. Lewis**, **C. L. Schauer**, **G. A. Sotzing**, **S. E. Stitzel**, **T. P. Vaid**, and **D. R. Walt**: Cross-Reactive Chemical Sensor Arrays, *Chemical Reviews 100*(7):2595–2626 (2000).

[34] **Wang, C.**, **L. Yin**, **L. Zhang**, **D. Xiang**, and **R. Gao**: Metal oxide gas sensors: Sensitivity and influencing factors, *Sensors 10*(3):2088–2106 (2010).

[35] **Prudenziati, M.** and **B. Morten**: Thick-film sensors: An overview, *Sensors and Actuators 10*(1):65–82 (1986).

[36] **Sekhar, P. K.**, **J. Kysar**, **E. L. Brosha**, and **C. R. Kreller**: Development and testing of an electrochemical methane sensor, *Sensors and Actuators B: Chemical 228*(Supplement C):162 – 167 (2016).

[37] **Karpov, E. c.**, **c. F. Karpov**, **c. Suchkov**, **S. Mironov**, **A. Baranov**, **V. Sleptsov**, and **L. Calliari**: Energy efficient planar catalytic sensor for methane measurement, *Sensors and Actuators A: Physical 194*(Supplement C):176 – 180 (2013).

[38] **Chiu, S.-W.** and **K.-T. Tang**: Towards a Chemiresistive Sensor-Integrated Electronic Nose: A Review, *Sensors 13*(10):14214–14247 (2013).

[39] **van den Bossche, M.**, **N. T. Rose**, and **S. F. J. D. Wekker**: Potential of a low-cost gas sensor for atmospheric methane monitoring, *Sensors and Actuators B: Chemical 238*(Supplement C):501 – 509 (2017).

[40] **Barsan, N.**, **M. Schweizer-Berberich**, and **W. Göpel**: Fundamental and practical aspects in the design of nanoscaled SnO2 gas sensors: A status report, *Fresenius' Journal of Analytical Chemistry 365*(4):287–304 (1999).

[41] **Ahlers, S.**, **G. Müller**, and **T. Doll**: A rate equation approach to the gas sensitivity of thin film metal oxide materials, *Sensors and Actuators B: Chemical 107*(2):587–599 (2005).

[42] **Williams, T.** and **C. Kelley**: Gnuplot 5.0: An Interactive Plotting Program (2016).

[43] **Benkstein, K. D.**, **P. H. Rogers**, **C. B. Montgomery**, **C. Jin**, **B. Raman**, and **S. Semancik**: Analytical capabilities of chemiresistive microsensor arrays in a simulated Martian atmosphere, *Sensors and Actuators B: Chemical 197*(Supplement C):280 – 291 (2014).

[44] **Solis, J. L.**, **G. E. Seeton**, **Y. Li**, and **L. B. Kish**: Fluctuation-enhanced multiple-

gas sensing by commercial Taguchi sensors, *IEEE Sensors Journal 5*(6):1338–1345 (2005).

LIST OF FIGURES

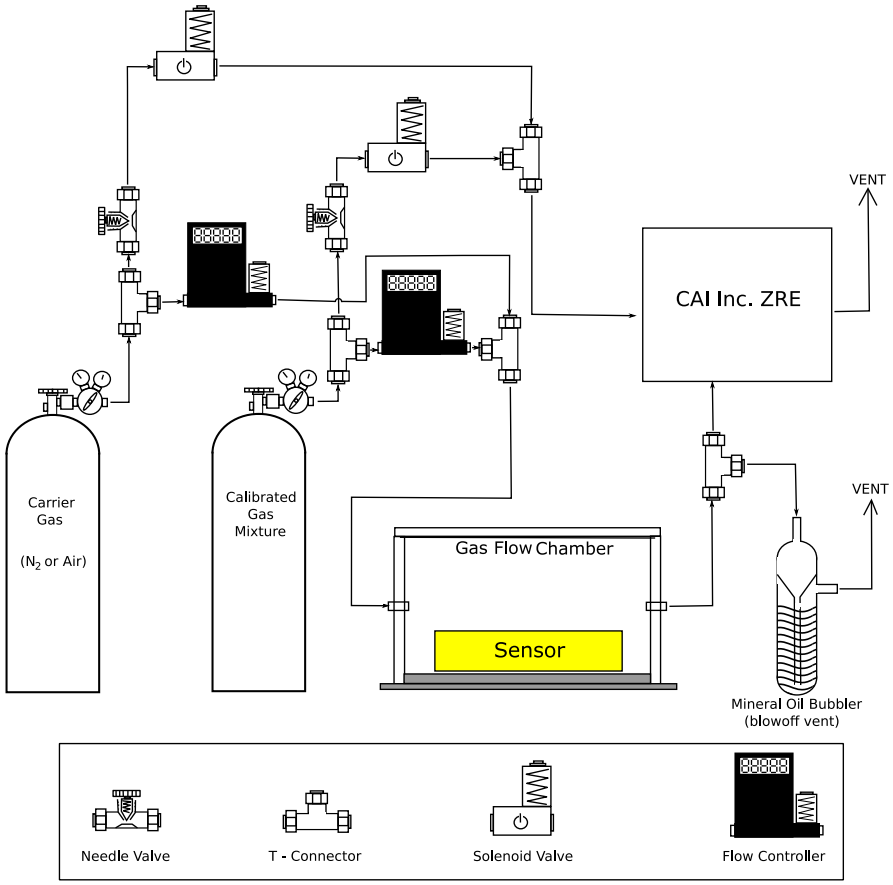

Figure 1. Component diagram of the gas mixing apparatus with chamber (Gas Flow Chamber) for diffusion-based sensors. The flow controllers allows mixing of the gases from the Calibrated Gas Mixture and Carrier Gas cylinders. After mixing, the analyte gas passes through the gas flow chamber(s) (more detail provided Figure 2) and flows next into the ZRE Non-Dispersive Infrared Analyzer, California Analytical Instruments, Inc., Orange, CA for analysis. This system provides a high accuracy measurement of analyte gas concentration, calibrated directly using solenoid valves from the carrier gas (zero) and mixture gas (span) cylinders.

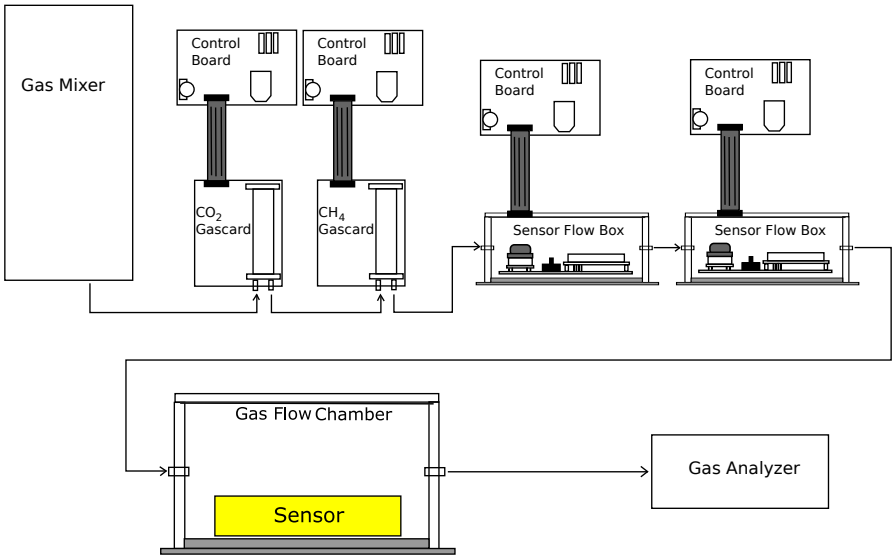

Figure 2. The diagram shows the flow of gas from the mixing apparatus to Gascard sensors, small enclosures containing sensors, the large gas flow chamber, and finally to the ZRE Non-Dispersive Infrared Analyzer, California Analytical Instruments, Inc., Orange, CA. The gas mixing apparatus is shown in Figure 1. The reported concentrations are based on the value detected by the ZRE Non-Dispersive Infrared Analyzer, California Analytical Instruments, Inc., Orange, CA.

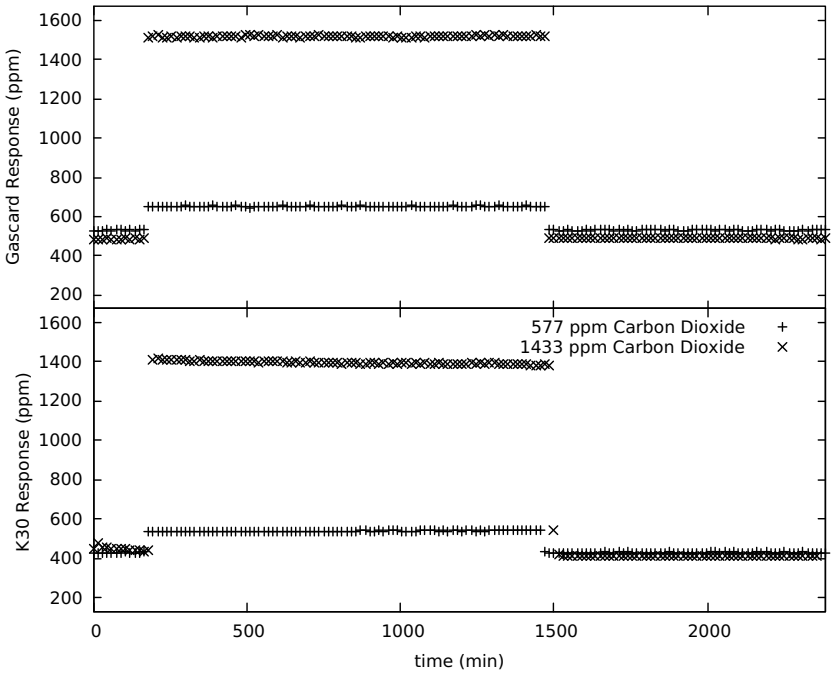

Figure 3. The Gascard (top) and K-30 (bottom) sensor response over time at high (1433 ppm, plotted with "×" on the plot) and low (577 ppm, plotted with "+") concentrations of carbon dioxide. The reported concentrations (577 and 1433 ppm) were determined by the ZRE Non-Dispersive Infrared Analyzer, California Analytical Instruments, Inc., Orange, CA.

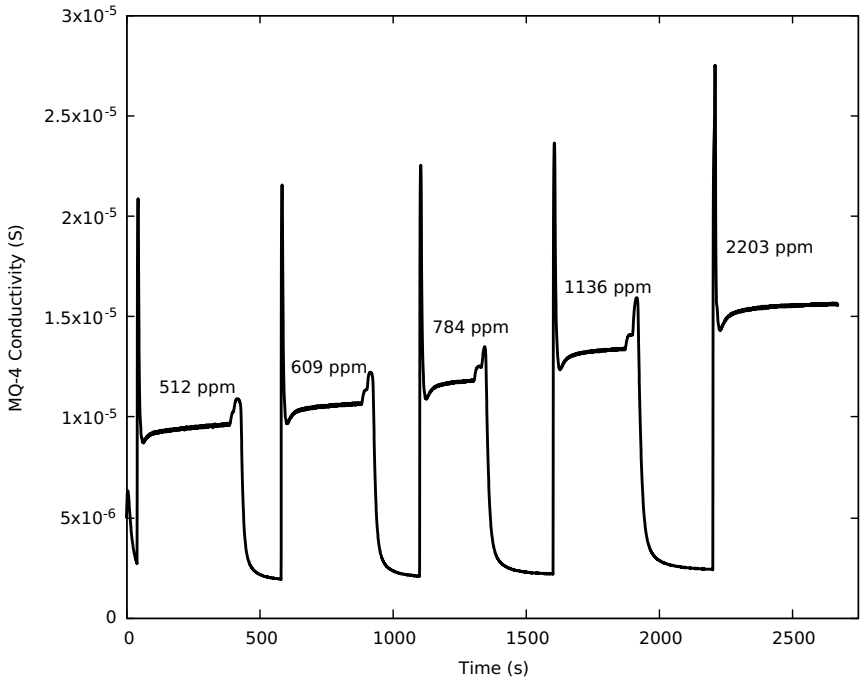

Figure 4. The conductive response of the MQ-4 at different methane concentrations between 500 and 2200 ppm. At the introduction of gas for each concentration change, a significant overshoot in conductivity is observed. The sensor showed noticeable delay between introduction of gas (the sharp increases in conductivity) and production of a stable response. The reported concentrations are based on the value detected by the ZRE Non-Dispersive Infrared Analyzer, California Analytical Instruments, Inc., Orange, CA.

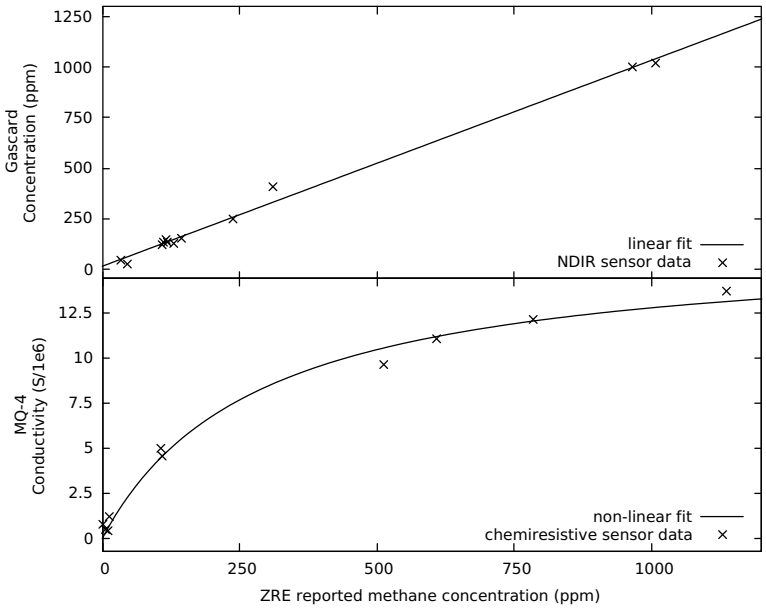

Figure 5. The response of the Gascard and MQ-4 sensors with respect to the concentration reported from the California Analytical Instruments Inc. ZRE Non-Dispersive Infrared Analyzer for different concentrations of either carbon dioxide or methane, respectively. The top part of the figure shows the response of an optical carbon dioxide sensor (Gascard, units were reported by the sensor as a fraction of the 50,000 ppm span, necessitating the units of this axis in terms of ppm) with the expected linear behavior. The bottom part of the figure shows the response of a chemiresistive methane sensor (MQ-4, response is expressed in conductivity observed directly from the sensor element) with a fit to the non-linear response

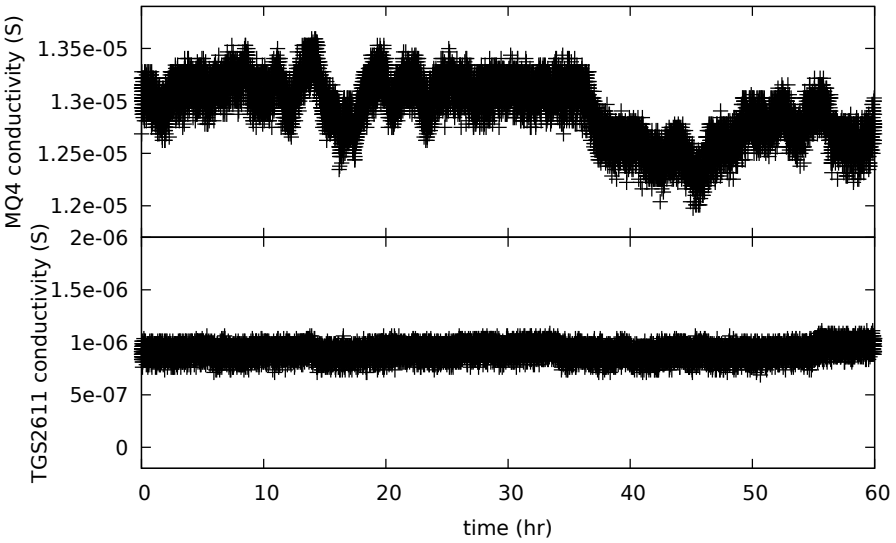

Figure 6. Long term baseline data were collected at the atmospheric baseline conditions (using a bottle of compressed medical grade breathing air (approximately 0 ppm methane), in the gas mixing chamber. The baseline fluctuations can be observed in these plots.

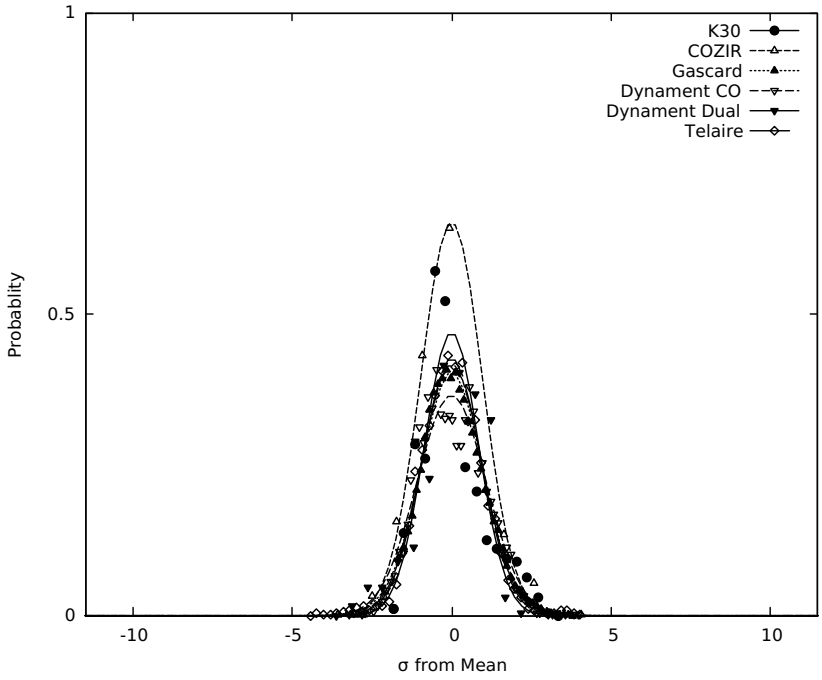

Figure 7. Frequency distribution of the digitized sensor output around the mean response of the sensor (points), along with Gaussian non-linear for each carbon dioxide sensors around the typical environmental baseline concentration of 400 ppm. Any deviation between the center of the Gaussian fit and the mean are due to significant asymmetry of the frequency distribution around the mean.

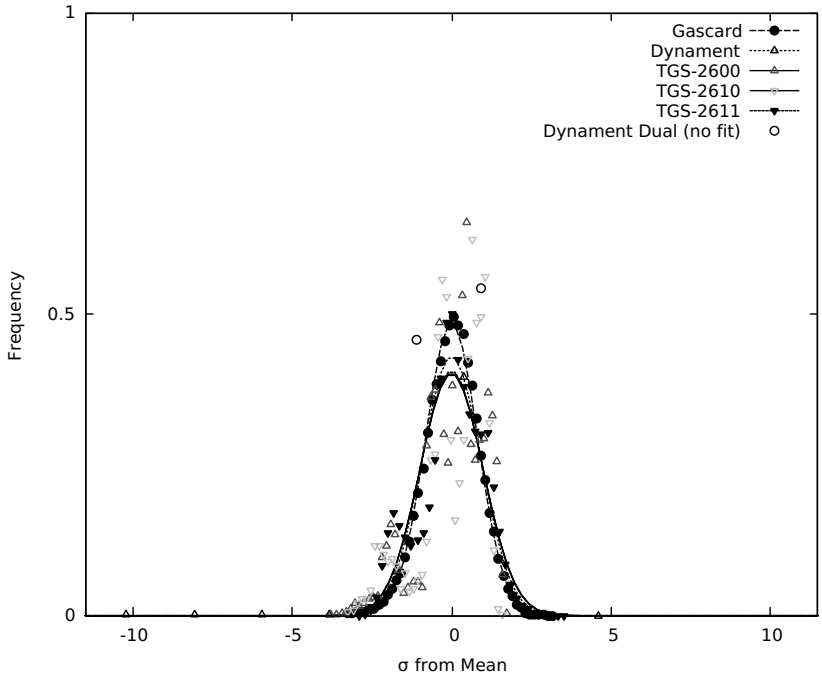

Figure 8. Frequency distribution of the digitized sensor output around the mean response of the sensor (points), along with Gaussian non-linear fit for each methane sensor around the typical environmental baseline concentration of 0 ppm. Any deviation between the center of the Gaussian fit and the mean are due to significant asymmetry of the frequency distribution around the mean.

LIST OF TABLES

Table 1: Manufacturer information of evaluated carbon dioxide sensors

Sensor	Supplier	Location
K-30 SE-0018	CO2Meter Inc.	Ormond Beach, FL
COZIR AMB GC-020	CO2Meter Inc.	Ormond Beach, FL
Gascard CO_2	Edinburgh Instruments Ltd.	Livingston, UK
MSH-P/CO2/NC/5/V/P/F	Dynament Ltd.	Mansfield, UK
MSH-DP/HC/CO2/NC/P/F	Dynament Ltd.	Mansfield, UK
Telaire T6615	Amphenol Advanced Sensors	St. Marys, PA

Table 2: Manufacturer information of evaluated methane sensors

Sensor	Supplier	Location
MQ-4	Futurelec	New York, NY
Gascard CH_4	Edinburgh Instruments Ltd.	Livingston, UK
MSH-P/HC/NC/5/V/P/F	Dynament Ltd.	Mansfield, UK
MSH-DP/HC/CO2/NC/P/F	Dynament Ltd.	Mansfield, UK
TGS-2600	Figaro Engineering Inc.	Osaka, Japan
TGS-2610	Figaro Engineering Inc.	Osaka, Japan
TGS-2611	Figaro Engineering Inc.	Osaka, Japan

Table 3. Nominal makeup of gas mixtures from Airgas Inc. (certified to ±2% of the stated values) used to prepare various gas mixtures in this study. The balance gas represents the gas present in addition to the parts-per-million concentrations of carbon dioxide and methane.

Carbon Dioxide	Methane	Balance Gas
3000 ppm	3000 ppm	nitrogen
100 ppm	100 ppm	nitrogen
0 ppm	20 ppm	nitrogen

Table 4. Standard deviation of gaussian fitted probability distributions and root-mean-squared error

	Sensor	σ_{GAUSS} (ppm)	RMSE
Carbon Dioxide	K-30 SE-0018	1.91	0.219
	COZIR AMB GC-020	14.1	0.304
	Gascard CO_2	2.12	0.223
	MSH-DP/HC/CO2/	86.4	0.197
	MSH-P/CO2/	17.6	0.217
	Telaire T6615	4.42	0.185
Methane/Hydrocarbon	MQ-4	0.48[†]	
	Gascard CH_4	35.7	0.222
	MSH-P/HC/	3.54	0.152
	TGS-2600	1.56	0.225
	TGS-2610	9.69	0.237
	TGS-2611	0.25	0.208

[†] This value was determined directly from the experimental response. See text.

Table 5: IUPAC and calibration corrected limits of detection in ppm

	Sensor	IUPAC (3σ)	Corrected[†]
Carbon Dioxide	K-30 SE-0018	5.7	25
	COZIR AMB GC-020	42	74
	Gascard CO_2	6.5	54
	MSH-DP/HC/CO2/	260	280
	MSH-P/CO2/	53	76
	Telaire T6615	13	27
Methane	MQ-4	53	82
	Gascard CH_4	110	151
	MSH-P/HC/	11	170
	TGS-2600	74	120
	TGS-2610	74	110
	TGS-2611	11	16

[†] A linear calibration was used for the optical sensor, while the chemiresistive used the non-linear Langmuirian fit. See text.